International Journal of Multiphase Flow 36 (2010) 825–835

Contents lists available at ScienceDirect

International Journal of Multiphase Flow

journal homepage: www.elsevier.com/locate/ijmulflow

Planar laser-induced fluorescence (PLIF) measurements of liquid film thickness in annular flow. Part II: Analysis and comparison to models

D. Schubring [a,b,*], T.A. Shedd [b], E.T. Hurlburt [c]

[a] Visualization, Imaging, and Computation of Thermohydraulics for Reactors (VICTR) Lab, University of Florida, 202 Nuclear Science Building, P.O. Box 118300, Gainesville, FL 32611-8300, USA
[b] Multiphase Flow Visualization and Analysis Laboratory (MFVAL), University of Wisconsin-Madison, 1500 Engineering Drive, Madison, WI 53706-1609, USA
[c] Bettis Laboratory West Mifflin, PA 15122, USA

ARTICLE INFO

Article history:
Received 22 September 2009
Received in revised form 23 December 2009
Accepted 12 February 2010
Available online 20 February 2010

Keywords:
Film thickness
Vertical flow
Annular flow
Fluorescence

ABSTRACT

Film thickness distributions in upward vertical air–water annular flow have been determined using planar laser-induced fluorescence (PLIF). Film thickness data are frequently used to estimate interfacial shear and pressure loss. This film roughness concept has been used in a number of models for annular flow of varying complexity. The PLIF data are presently applied to the single-zone interfacial shear correlation of Wallis; the more detailed model of Owen and Hewitt; and the two-zone (base film and waves) model of Hurlburt, Fore, and Bauer. For the present data, these models all under-predict the importance of increasing liquid flow on pressure loss and interfacial shear. Since high liquid flow rates in annular flow induce disturbance wave and entrainment activity, further modeling in these areas is advised.

1. Introduction

In industrial heat transfer applications with two-phase flow, the annular regime is among those of foremost interest due to the large number of systems and wide range of flow qualities in which it is seen. As discussed in Part I: Methods and Data (Schubring et al., submitted for publication), typical modeling of annular flow is based on the film roughness concept, part of the triangular relationship asserted by Hewitt and Hall Taylor (1970). The liquid film is conceptualized to present a roughened surface to the gas core that enhances interfacial shear and pressure losses. Single-zone roughness models dominate the literature; a linear relationship between effective roughness and average film thickness is often employed.

Visualizations of the film indicate the actual roughness is not at all homogeneous. Instead, a major source of roughness is intermittent disturbance waves. Hewitt et al. (1990), observing this behavior, suggested an intermittently rough interface instead. Direct inspection of the images from (Schubring et al., submitted for publication) confirms these observations. More recently, researchers such as Wang et al. (2004) have suggested that wave characteristics such as their velocity and frequency must be explicitly considered in order to correlate interfacial friction factors. A number of studies of disturbance waves have been performed. Various early efforts are discussed in the reviews of Azzopardi (1986, 1997). More recent work includes that by the present authors (Schubring and Shedd, 2008; Schubring et al., 2010) and Sawant et al., 2008.

There are several motivations for moving to a multi-zone film modeling approach in annular flow. Physically, the film of annular flow shows multiple types of behavior, with the sharpest distinction between base film and disturbance waves. The model of Hurlburt et al. (2006) was motivated in large part by a desire to accurately model two-phase annular flow at high-pressures, where the phase density and velocity ratios are diminished over the present low-pressure data.

More generally, if base film and disturbance waves do display fundamentally different roughness/shear behaviors – as suggested by Hewitt et al. (1990) – a physical model of annular flow must account for this. Such a physical model would provide not only average shear, as would a correlation such as Wallis (1969), but shear in both zones. As a result, base film average shear (to which most of the tube is exposed) and wave zone shear (to which waves are exposed and from which droplets are entrained) can be quantified separately. A model of the liquid flow in the film (*e.g.*, assessment of any turbulence that might be present) is likely to require this time/space resolved shear data rather than merely the average.

In Part I, planar laser-induced fluorescence (PLIF) measurements of film thickness distribution were discussed. These measurements can be used to evaluate correlations/models of annular flow that rely on the film roughness concept. The single-

* Corresponding author. Address: Visualization, Imaging, and Computation of Thermohydraulics for Reactors (VICTR) Lab, University of Florida, 202 Nuclear Science Building, P.O. Box 118300, Gainesville, FL 32611-8300, USA. Tel.: +1 352 392 1401x314; fax: +1 352 392 3380.
E-mail address: dlschubring@ufl.edu (D. Schubring).

0301-9322/$ - see front matter © 2010 Elsevier Ltd. All rights reserved.
doi:10.1016/j.ijmultiphaseflow.2010.02.002

zone models of Wallis (1969) and Owen and Hewitt (1987) are considered. The techniques used to divide measurements between base film and waves are then described, followed by their application to the recent two-zone model of Hurlburt et al. (2006). The accuracy of these models and the applicability of the underlying film roughness concept are investigated through comparison of predicted and experimental interfacial shear. The goal of the present paper is not to evaluate all possible pressure loss (or other) models for annular flow, but rather to focus on the film roughness concept through the new film thickness distribution data.

Based on these results, recommendations for further improvements in annular flow modeling are then presented.

2. Experimental

A vertical flow facility (Fig. 1) was constructed with a 22.4 mm ID fluorinated ethylene propylene (FEP) test section to allow for visualization of thin films near the wall. Measurements of flow rates, absolute test section pressure, and pressure gradient were made in a similar 23.4 mm ID quartz test section and adjusted to account for the change in tube diameter. Gas meter readings ($Q_{g,nom}$ – standard liters per minute) between 800 and 1600 L min^{-1} (0.0133–0.0267 standard m^3 s^{-1}) were considered in 200 L min^{-1} increments. Uncertainties were estimated at 70 L min^{-1} at and below 1400 L min^{-1} flow and 100 L min^{-1} for 1600 L min^{-1} flows. Superficial gas velocities (U_{sg}) ranged from 35–85 m s^{-1}. Liquid flow rates of 1.5–8 L min^{-1} were studied, corresponding to liquid superficial velocities (U_{sl}) of 6–34 cm s^{-1}, with an estimated 5% uncertainty. Pressure gradient (dP/dx) and wall shear (τ_w) are estimated with a 5–10% uncertainty (highest for low flow rates).

A schematic of the test section and optics is shown in Fig. 2. The FEP test section was surrounded by a water-filled box, painted black except for viewing windows, to enhance the optical signal-to-noise ratio. The PLIF measurements required a Nd:YAG laser, fluorescing Rhodamine B dye in the water, and a CCD camera with a red filter for observation of the resulting fluorescence. The camera lens used produced square pixels 3.14 μm on a side (4 mm total axial length per image).

Additional details regarding the flow facility and optical apparatus are provided in Schubring et al. (submitted for publication).

3. Application to single-zone models

A number of single-zone film roughness models for annular flow exist, most centering on a simple explicit linear expression for shear at the gas–liquid interface, τ_i, as a function of average film thickness, δ. A simple model, that of Wallis, and a more complex model, that of Owen and Hewitt, are considered.

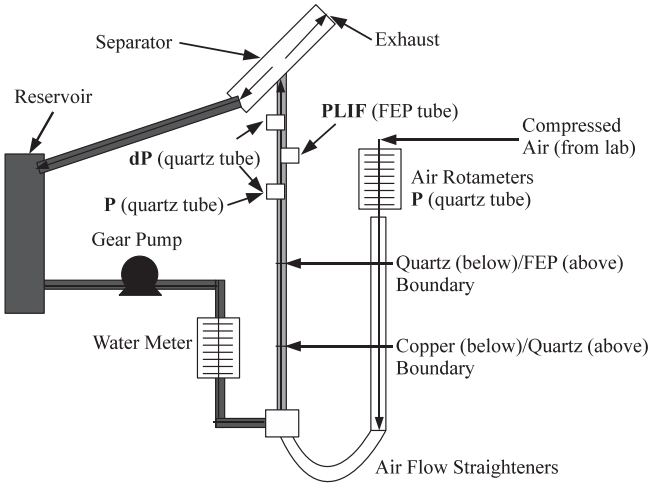

Fig. 1. Diagram of flow loop.

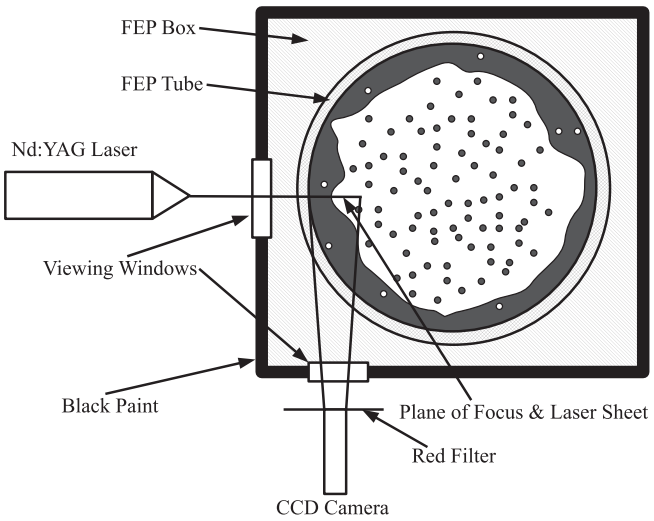

Fig. 2. Test section for PLIF measurements. Flow is out of the plane of the page.

3.1. Application of Wallis model

The Wallis correlation most often used is shown in Eq. (1). In the original Wallis correlation, the factor of $0.079Re_g^{-0.25}$ (the Blasius friction factor) was instead a constant of 0.005.

$$\tau_{i,Wallis} = 0.079Re_g^{-0.25}KE_{sg}\left(1+300\frac{\delta}{D}\right) \tag{1}$$

The experimental interfacial shear, τ_i, is estimated as suggested by Fore et al. (2000):

$$\tau_i = -\frac{D-2\delta}{4}\left(1-\frac{\rho_{core}U_g^2}{P_{abs}}\right)\frac{dP}{dx} - \rho_{core}g\frac{D-2\delta}{4} - R_D(U_D-U_E) \tag{2}$$

$$U_g = \left(\frac{D}{D-2\delta}\right)^2 U_{sg} \tag{3}$$

In this equation, R_D is the rate of droplet deposition (assumed equal to the rate of droplet entrainment), with U_D and U_E as the velocities of depositing and entraining droplets. That is, the entrainment is assumed to be fully developed and any developing flow effects are not considered in this equation. Based on visualizations of annular flow and the CFD simulation of Han (2005), most droplets are entrained from waves. Therefore, the wave velocity (v_{wave}) can be used in place of U_E. ρ_{core} is the core density, with P_{abs} as the absolute test section pressure and U_g as the actual average gas velocity (considering the effective area of the gas core).

The Universal Velocity Profile (UVP – Eq. (4)) from turbulent, wall-bounded flow is assumed within the film:

$$u^+ = \begin{cases} y^+ & \text{if } y^+ < 5 \\ -3+5\ln(y^+) & \text{if } 5 < y^+ < 30 \\ 5.5+2.5\ln(y^+) & \text{if } 30 < y^+ \end{cases} \tag{4}$$

The UVP is non-dimensionalized in wall coordinates (u^+ and y^+), which are defined using the following equations:

$$u^+(y) = \frac{u(y)}{u_l^\star} \tag{5}$$

$$y^+ = \frac{y u_l^\star}{\nu_l} \tag{6}$$

$$u_l^\star = \sqrt{\frac{\tau_i}{\rho_l}} \tag{7}$$

$$\delta^+ = \frac{\delta u_l^\star}{\nu_l} \tag{8}$$

In these equations, ν_l is the kinematic viscosity of water. A dimensionless film flow rate, $\dot{m}^+_{l,film,OH}$, is defined as follows, with μ_l as the dynamic viscosity of water:

$$\dot{m}^+_{l,film} = \frac{\dot{m}_{l,film}}{\pi D \mu_l} \tag{9}$$

By integrating the UVP, the dimensionless flow rate can be related to the film height:

$$\dot{m}^+_{l,film,OH} = \begin{cases} 0.5(\delta^+)^2 & \text{if } \delta^+ < 5 \\ -64 + 3\delta^+ + 2.5\delta^+ \ln(\delta^+) & \text{if } 5 < \delta^+ < 30 \\ 12.05 - 8.05\delta^+ + 5\delta^+ \ln\left(\delta^+\right) & \text{if } 30 < \delta^+ \end{cases} \tag{10}$$

Entrained fraction, E, is then estimated using a mass balance:

$$E = \frac{\dot{m}_{l,Ent}}{\dot{m}_l} = \frac{1 - \dot{m}_{l,film}}{\dot{m}_l} \tag{11}$$

The model for τ_i also relies on R_D, the droplet deposition rate. A correlation for R_D is obtained from Ishii and Mishima (1981). The dependence of τ_i on this correlation is weak; given a droplet deposition rate between zero and twice that predicted by the correlation, τ_i results vary by less than 10%. The estimate for R_D (along with core void fraction, α_{core}; core droplet mass concentration, $\rho_{l,core}$; and a one-zone mean gas velocity, U_g) is found by solving the following coupled equations:

$$R_D = \rho_{l,core} k_{mass,Ent} \tag{12}$$

$$\rho_{l,core} = \frac{\rho_l U_{sl} E U_g}{U_{sg} U_{l,core} + U_{sl} E U_g} \tag{13}$$

$$k_{mass,Ent} = 0.022 U_{sg} Re_g^{-0.25} \left(\frac{\rho_g}{\rho_{l,core}}\right)^{0.26} \tag{14}$$

$$Re_g = \frac{\rho_g U_{sg} D}{\mu_g} \tag{15}$$

$$U_g = U_{sg} \left(\frac{D}{D - 2\bar{\delta}}\right)^2 \frac{1}{\alpha_{core}} \tag{16}$$

$$\frac{\dot{m}_g}{E\dot{m}_l} = \frac{U_g}{U_{l,core}} \frac{\rho_g}{\rho_l} \frac{\alpha_{core}}{1 - \alpha_{core}} \tag{17}$$

The velocity of liquid droplets in the core, $U_{l,core}$ and liquid droplets depositing back into the film, U_D, are assumed equal to the velocity of the gas in the core (homogeneous model) for simplicity. The overall model performance is only weakly dependent on these details (τ_i changes by less than 2% for droplet-gas slip ratios of 1–3 in the core).

Assuming that the entrained fraction, E, from the model is accurate, the uncertainty on interfacial shear is estimated at 5–10%, dominated by uncertainty on pressure loss. This uncertainty includes that on R_D (more specifically, on $k_{mass,Ent}$, assumed to be a factor of two. Additional uncertainty on τ_i due to E is difficult to estimate. However, if the range of E is taken (very conservatively) as from 0 (no entrainment) to 1 (full entrainment), a total average uncertainty on τ_i of 15% is estimated (lower for low gas flows, slightly higher for high gas flows).

A useful way to compare the agreement of a correlation or model is with mean absolute error (MAE), defined as below for a number of flow conditions, n_{FC}, modeled result XX_{mod}, and experimental result XX_{exp}.

$$\text{MAE} = \frac{1}{n_{FC}} \sum_{FC} \left| \frac{XX_{corr} - XX_{exp}}{XX_{exp}} \right| \times 100\% \tag{18}$$

For the present data, a mean absolute error (MAE) for the Wallis correlation of 22.7% is found. (If the original constant of 0.005 is used instead of the Blasius friction factor, an MAE of 22.6% is obtained instead.) The agreement is shown in Fig. 3. Prediction for low liquid flows is strong. For the highest liquid flow series shown, the Wallis correlation predicts a weak and non-monotonic trend with gas flow; this contrasts sharply with the increase seen in the experimental data.

This indicates that the behavior of annular flow with high liquid flow rate is not predicted accurately by the Wallis correlation. While pressure loss (interfacial shear) is a strong function of liquid flow rate, gas kinetic energy and average film thickness are not. High liquid flow annular flows are characterized by disturbance waves and high entrained mass flow rates; these results suggest that one (or both) of these areas must be modeled in more detail.

3.2. Outline of Owen and Hewitt model

A more complex model, that of Owen and Hewitt (1987), is also selected for consideration. This model, as originally presented, computes film height and pressure loss given entrained fraction, E, the fraction of total liquid flow found in the gas core (as opposed to the film). By solving the equations of the model with δ as known instead of E (suggested by Rodríguez (2004)), estimates of entrained fraction and pressure loss are obtained as outputs. The model is composed of liquid film and gas core sub-models and is outlined below.

The liquid film sub-model requires the interfacial shear ($\tau_{i,OH}$) and the film flow rate ($\dot{m}_{L,film,OH}$) and estimates the interfacial velocity and film thickness. The characteristic shear, τ_{OH}, in the film is defined by averaging $\tau(y)$, obtained by a force balance, in the film. This can be solved analytically based on the expressions in the paper, using D (tube diameter), ρ_l (liquid density), and g (the acceleration due to gravity):

$$\tau_{OH} = \tau_{i,OH} \frac{D - 2\delta}{D} - \left(\frac{dP}{dx} + \rho_l g\right) \left[\frac{\delta D}{2} - \frac{\delta^2}{3}\right] \tag{19}$$

The second output of the film model, the interfacial velocity, $U_{l,i,OH}$, is found by evaluating the UVP at a y^+ of δ^+. In the Owen and Hewitt model, the characteristic shear (τ_{OH}) is used instead of the interfacial shear, τ_i.

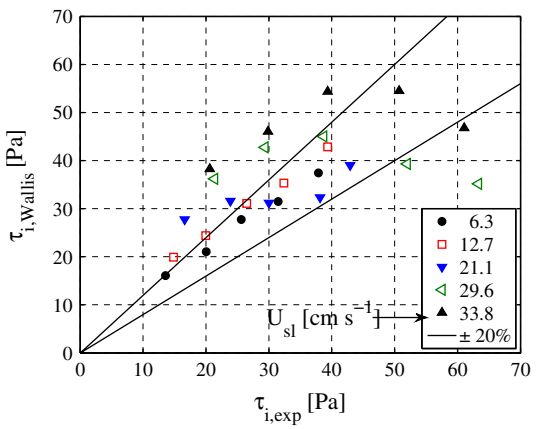

Fig. 3. Performance of Wallis correlation with respect to interfacial shear, τ_i.

The gas core sub-model proceeds as follows. The entrained droplet mass flow rate ($\dot{m}_{l,Ent,OH}$) along with the core diameter (D_{core}), area (A_{core}), density (ρ_{core}), and velocity ($U_{Core,h,OH}$) are found using a homogeneous model of the gas and liquid droplets in the core. In these equations, $\dot{m}_g$, ρ_g, and $\dot{m}_l$ refer to the gas mass flow rate, gas density, and liquid mass flow rate, respectively.

$$D_{core} = D - 2\delta \tag{20}$$

$$A_{core} = \frac{D_{core}^2 \pi}{4} \tag{21}$$

$$\dot{m}_{l,Ent,OH} = \dot{m}_l - \dot{m}_{l,film,OH} \tag{22}$$

$$\rho_{core} = \left(\dot{m}_g + \dot{m}_{l,Ent,OH}\right)\left(\frac{\dot{m}_g}{\rho_g} + \frac{\dot{m}_{l,Ent,OH}}{\rho_l}\right)^{-1} \tag{23}$$

$$U_{core,h,OH} = \frac{1}{A_{core}}\left(\frac{\dot{m}_g}{\rho_g} + \frac{\dot{m}_{l,Ent,OH}}{\rho_l}\right) \tag{24}$$

By assuming ideal gas behavior in the gas, incompressible behavior in the liquid droplets, and no axial variation in entrained fraction or film thickness, Owen and Hewitt's equation for interfacial shear can be simplified to (with P_{abs} as the absolute pressure in the test section):

$$\tau_{i,OH} = -\frac{D_{core}}{4}\left(1 - \frac{\rho_{core} U_{core,h,OH}^2}{P_{abs}}\right)\frac{dP}{dx} - \frac{D_{core}}{4}\rho_{core} g \tag{25}$$

The modeled interfacial Fanning friction factor, $C_{f,i,OH}$, is defined as:

$$C_{f,i,OH} = \frac{2\tau_{i,OH}}{\rho_{core}\left(U_{core,h,OH} - U_{l,i,OH}\right)^2} \tag{26}$$

For the two-phase case, the following adaptation of the Nikuradse equation is derived:

$$\sqrt{\frac{2}{C_{f,i,OH}}} = \frac{1}{\kappa_{TP}}\ln\left(\frac{D_{core}}{2\epsilon_{eff,OH}}\right) + A_r - \frac{1.5}{\kappa_{TP}} + \frac{1}{\kappa_{TP}}\left[\frac{4\delta}{D}\ln\left(\frac{D}{2\delta}\right) - \frac{2\delta}{D}\right] \tag{27}$$

The symbol κ_{TP} is the two-phase von Kármán constant. A_r is a function of a roughness Reynolds number, $Re^\star$, related to the effective roughness, $\epsilon_{eff,OH}$, and the friction velocity.

The effective roughness is defined by:

$$\epsilon_{eff,OH} = \epsilon_{OH} - y_b \tag{28}$$

$$y_b = \frac{5.2D}{Re_g}\sqrt{\frac{2}{C_{f,g}}} \tag{29}$$

The gas core boundary sublayer (viscous sublayer) thickness, y_b, is defined by Owen and Hewitt as recommended by Nedderman and Shearer (1964). No explicit recommendation is provided by Owen and Hewitt for evaluation of $C_{f,g}$, a single-phase gas friction factor. The model is insensitive to the details of this evaluation. The Haaland (1983) correlation was used in present work with the same roughness ($\epsilon_{eff,OH}$) as in the rest of the Owen and Hewitt core model and a superficial gas Reynolds number, Re_g:

$$Re_g = \frac{4\dot{m}_g}{\pi D \mu_g} \tag{30}$$

$$\sqrt{\frac{1}{C_{f,g}}} = -3.6\log_{10}\left[\frac{6.9}{Re_g} + \left(\frac{\epsilon_{eff,OH}}{3.7D}\right)^{\frac{10}{9}}\right] \tag{31}$$

Three unknowns remain in the core model: κ_{TP}, A_r, and ϵ_{OH}. Owen and Hewitt correlated κ_{TP} graphically, which was provided as an explicit expression by Rodríguez (2004):

$$\kappa_{TP,corr} = 0.0918\left(\frac{\rho_g U_{sg}^2}{\rho_{core} U_{core,h,OH}^2}\right)^2 + 0.1186\frac{\rho_g U_{sg}^2}{\rho_{core} U_{core,h,OH}^2} + 0.1391 \tag{32}$$

The function A_r is also correlated graphically by Owen and Hewitt, as a function of the roughness Reynolds number, $Re^\star$, in turn a function of the friction velocity in the core, $u^\star_{core,OH}$:

$$Re^\star = \frac{\epsilon_{OH} u^\star_{core,OH} \rho_{core}}{\mu_h} \tag{33}$$

$$u^\star_{core,OH} = \sqrt{\frac{\tau_{i,OH}}{\rho_{core}}} \tag{34}$$

$$\mu_h = \left(\dot{m}_g + \dot{m}_{l,Ent,OH}\right)\left(\frac{\dot{m}_g}{\mu_g} + \frac{\dot{m}_{l,Ent,OH}}{\mu_l}\right)^{-1} \tag{35}$$

μ_g is the dynamic viscosity of the gas, used to compute the homogeneous (core) viscosity, μ_h.

For the range of $\log_{10}(Re^\star)$ that occurs in the present data (from 1.4 to 2.5), A_r is well-estimated from Owen and Hewitt's graphical correlation as:

$$A_r = \begin{cases} 11.5 - 1.5\log_{10}(Re^\star) & \text{if } \log_{10}(Re^\star) < 2 \\ 8.5 & \text{if } \log_{10}(Re^\star) > 2 \end{cases} \tag{36}$$

Finally, a relation between δ and ϵ_{OH} is required to close the model. Owen and Hewitt provide this graphically in a non-dimensional form, using:

$$\hat{\epsilon}_{OH} = \frac{2\epsilon}{D} \tag{37}$$

$$\hat{\delta}_{OH} = \frac{2\delta}{D} \tag{38}$$

$$We_{OH} = \frac{\rho_{core} U_{core,h,OH}^2 D_{core}}{\sigma} \tag{39}$$

$$Re_{l,film,OH} = \frac{\dot{m}_{l,film,OH} D}{A\mu_l} \tag{40}$$

For $\hat{\delta}_{OH}$ above 0.011, Owen and Hewitt recommend Fig. 10 in their paper, which correlates $\hat{\epsilon}_{OH}$ as a function of $\hat{\delta}_{OH}$ alone. At $\hat{\delta}_{OH}$ below 0.008, they note that this correlation is not appropriate and provide a relation that includes the effects of We_{OH} and $Re_{l,film,OH}$ A linear interpolation between the two results is employed between 0.008 and 0.011. Tabulated versions of these graphical correlations, developed by Rodríguez, were used to convert between $\hat{\delta}_{OH}$ and $\hat{\epsilon}_{OH}$.

3.3. Performance of Owen and Hewitt model

The one-to-one correspondence of δ and E allows the Owen and Hewitt model to be implemented as a film roughness correlation. In this mode, δ (from PLIF data) is used to predict both dP/dx and E. A scatterplot of modeled pressure loss and experimental data is shown in Fig. 4.

The MAE for the Owen and Hewitt film roughness correlation (with respect to dP/dx) is 17%. For low flow rates, the pressure loss prediction of Owen and Hewitt is acceptable, but the model diverges from reality rather strongly at higher flow rates. In particular, the trend of pressure loss with U_{sg} (at high total flow rate) is over-predicted (in sharp contrast with the Wallis model). Overall, the performance of this complex model is no better than that of some correlations that do not require film thickness information, such as those of Chisholm (1973) (15% MAE) and Müller-Steinhagen and Heck (1986) (13% MAE).

The Owen and Hewitt model, operating as a film roughness correlation, also produces an estimate of the entrained fraction, E, also shown in Fig. 4 with flow rates. Based on direct studies of entrainment in the literature and high-speed videos taken in the quartz

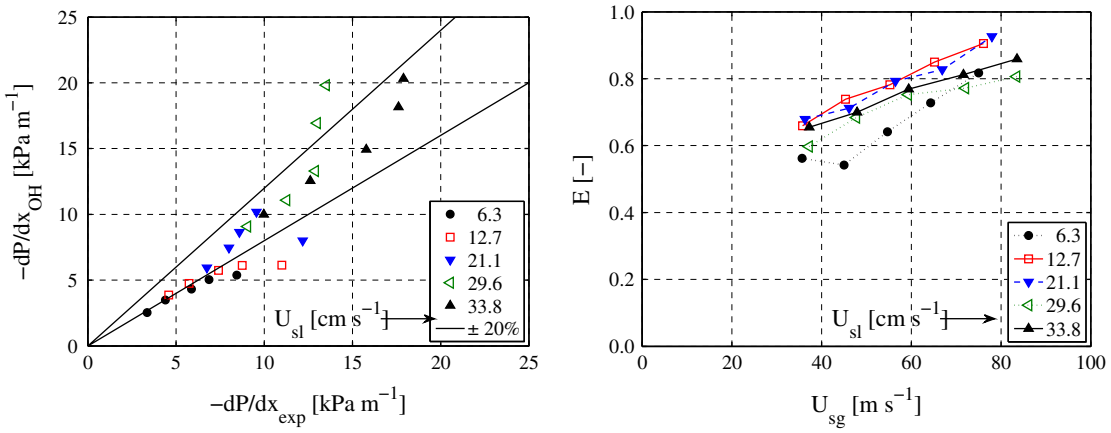

Fig. 4. Results of Owen and Hewitt model, phrased as a film roughness correlation. (Left) Agreement of dP/dx with experiment, series by U_{sl}. (Right) Estimates of liquid entrainment, series by U_{sl}.

test section, entrained fraction is expected to increase with gas flow rate. One recent study of this effect is that of ?, who studied entrained fraction with similar U_{sg}, U_{sl}, and P_{abs} as in the present study (though with a smaller tube). Entrainment was found to be a strong function of both gas and liquid flow rates within the range in the present study. (At higher pressure and therefore higher gas mass flow rate, an asymptotic effect of $E(U_{sg})$ was found.) Entrained fractions of 0.1–0.7 are found.

An increase in E with U_{sg} is seen in the modeled results, but the dependence is weaker than would be expected based on the literature. Perhaps more alarmingly, the dependence of entrained fraction on liquid flow is weak and non-monotonic. Finally, the values of E are very high for high flow qualities (greater than 0.9), which also does not watch the results of Sawant et al., 2008.

It is possible to use both δ and dP/dx as inputs if one relation in the model is ignored, such as that between δ and ϵ. When this is done, the experimental value of δ is used for determination of core geometry and film flow rate, while ϵ is determined from the required friction factor to match dP/dx.

The comparison between δ and this closure ϵ is shown in Fig. 5. These plots show that ϵ is not a function of δ alone; the effect of liquid flow rate must be considered. The Owen and Hewitt model advises such a consideration for thin films (high gas flows), but these plots demonstrate that liquid flow rate must be considered for all gas flow rates in the present databank. Fig. 5 also shows a plot of the standard deviation of film thickness ($s(\delta)$) against the closure ϵ that also shows a dependence of ϵ on liquid flow. That is, higher liquid flow rates would require a larger roughness for the same average film thickness. Such a roughness may be linked to the presence of additional disturbance waves along the film-core interface.

Another possible shortcoming is the homogeneous model in the core. In equilibrium annular flow, droplets are usually conceptualized as being in a dynamic equilibrium, with individual droplets continually entrained, accelerated, and redeposited. As a result, the mean droplet velocity may differ from the mean gas velocity in the core. Further, the net momentum exchange from the gas core to the film through droplets, which deposit at a higher velocity than that from which they were entrained, is not considered. The single-zone approach is also a limitation. The model of Hurlburt et al. (2006), discussed below, addresses both of these issues, but requires a division of film thickness data into base film and wave zones.

4. Base/wave division

To use PLIF measurements in a two-zone model, base film and wave height estimates must be separated. At least two methods for doing this have been suggested in the literature. The development of the model of Hurlburt et al. used conductance probe film thickness data. The base/wave division was accomplished by assuming all measurements above 1.1 times the average were waves, with those smaller modeled as base film. Applying this standard to the present data provides INT_w estimates ranging from

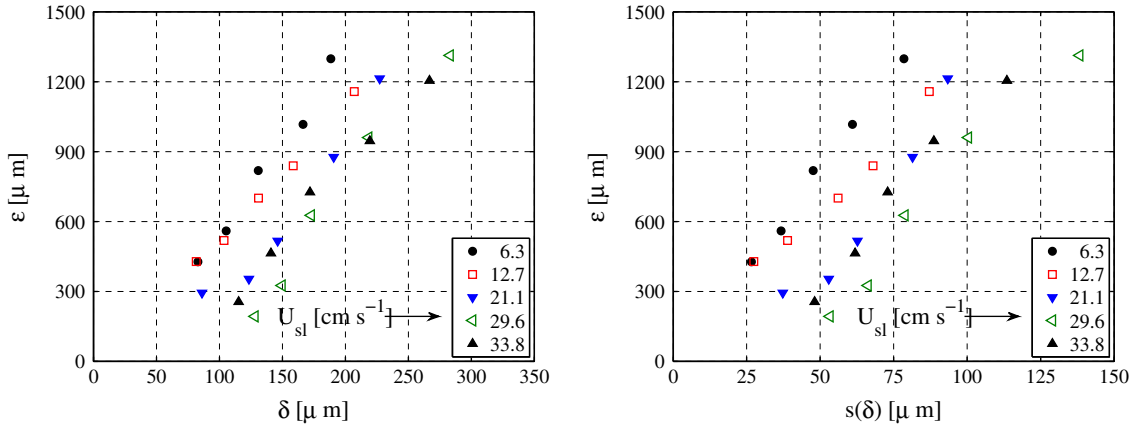

Fig. 5. Interfacial roughness, ϵ, to close Owen and Hewitt model given dP/dx and δ as inputs, series by U_{sl}. (Left) vs. δ. (Right) vs. $s(\delta)$.

30–40%, generally much larger than that seen with wave visualization (Fig. 11).

This division predicts an inverse relationship between INT_w and U_{sl}, which is not physical. Such a division could be generalized to a non-iterative criterion at a constant multiple of the average, or more generally to the sum of a constant times the average and a constant times the sample standard deviation. A wide range for these two constants was explored, but reasonable trends for INT_w were not obtained.

Using a similar PLIF setup, Rodríguez (2004) recommends division using a critical standard deviation multiplier, k_c. Film heights more than k_c standard deviations above the mean base film height are assumed to be waves. The MAE for this prediction is approximately 20% (for k_c of 2), relative to direct measurements of intermittency are available from Schubring et al. (2010), also shown in Fig. 11. INT_w is primarily a function of U_{sl}, with any link to gas flow weak and potentially non-monotonic.

Due to the lack of an objective base/wave division method, the results from Schubring et al. (2010) at the same meter readings (similar U_{sl} and U_{sg}) were employed. For the flow with $Q_{g,nom}$ of 800 L min^{-1} and Q_l of 8 L min^{-1}, INT_w is not available; the result from the immediately higher gas flow, $Q_{g,nom}$ of 1000 L min^{-1} and Q_l of 8 L min^{-1}, is employed instead. This approximation is reasonable as INT_w is predominantly a function of liquid flow.

Within each resulting zone, the average and standard deviation (along with their ratio) are shown in Fig. 6. The ratio of average

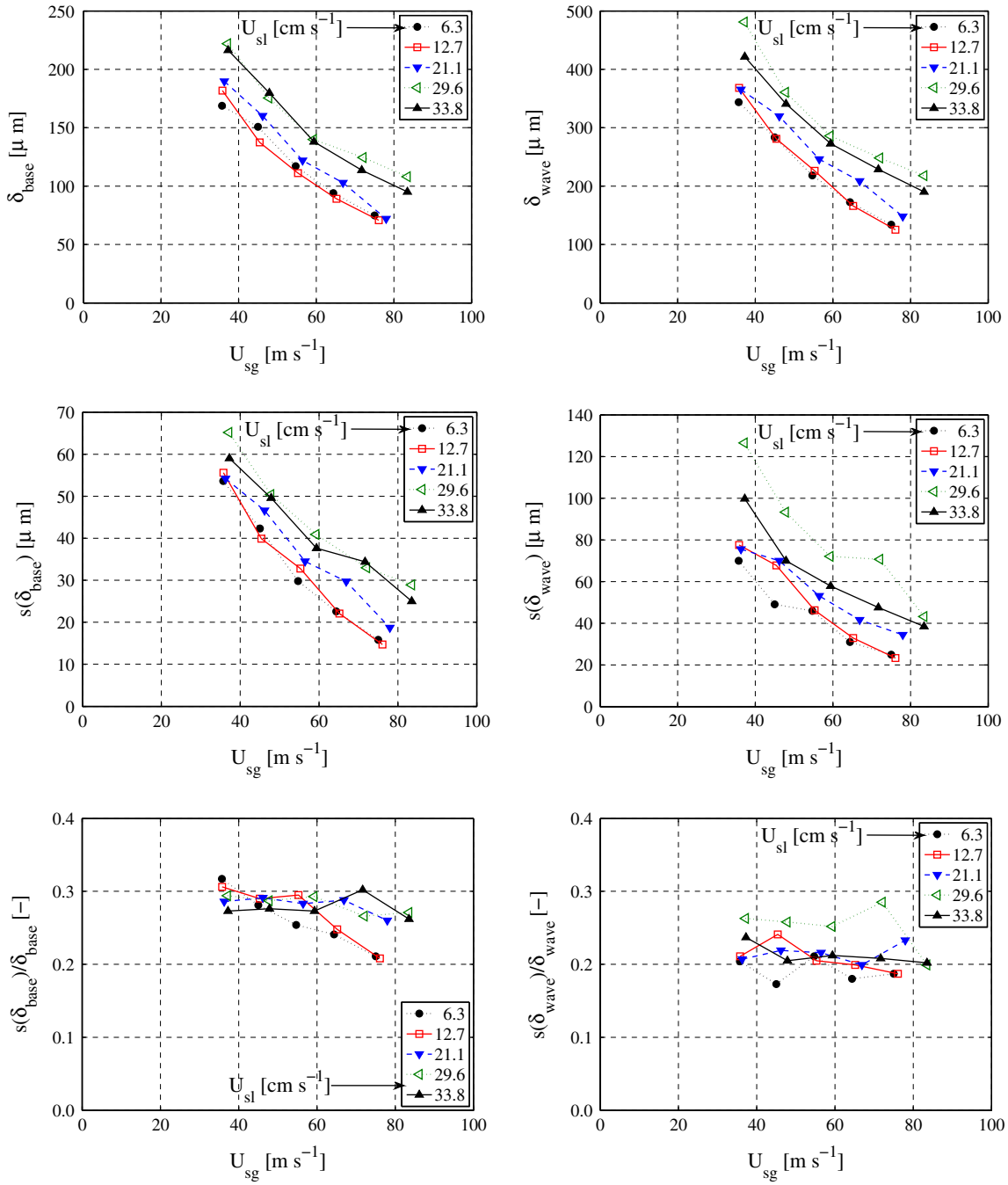

Fig. 6. Zone estimates of film thickness data vs. flow rates. (Left) Base film. (Right) Wave height. (Top) Average film thickness. (Middle) Standard deviation of film thickness. (Bottom) Their ratio.

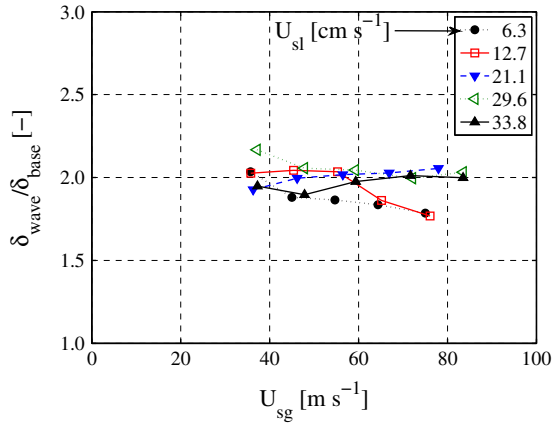

Fig. 7. Ratio of average wave height to average base film thickness vs. flow rates.

wave and base film heights is shown in Fig. 7. As with the single-zone measurements, the means and standard deviations (roughnesses) of base film thickness and wave height decrease with increasing gas flow and increase with increasing liquid flow. A nearly-constant roughness fraction ($s(\delta)/\delta$) is observed for both base film and waves at sufficient liquid flow; for waves, the roughness fraction appears constant even for low liquid conditions. The ratio of average wave heights and base film thicknesses also varies little across many of the flow conditions explored. A ratio of 2 is indicated to be a common characteristic of annular flow with sufficient liquid flow. This minimum liquid flow rate itself is an increasing function of gas flow, with series of constant liquid flow falling below the ratio of 2 at varying gas flow rates.

One explanation for this behavior is that liquid flow beyond the critical film flow rate (*i.e.*, that which can be supported by the base film alone) is transported by a mix of entrained droplets and disturbance waves. This critical film flow rate is at most a weak function of gas flow based on the experimental work of Asali (1984) and Schadel (1988). High-speed videos of wave behavior and direct studies of entrainment in the literature indicate that additional entrainment is expected at high gas flows, which may reduce the required wave height.

5. Application to two-zone model

Models that consider base film and waves separately (two-zone models) are relatively rare in the literature. One recent example, that of Hurlburt et al. (2006), was selected for consideration with the present data.

5.1. Outline of Hurlburt et al. model

The Hurlburt et al. model uses a roughness-modified log law to model interfacial shear. Based on experimental data (Jayawardena, 1993; Hay et al., 1996) are cited), the velocity profile within the gas core is well-modeled in this manner. In particular, the following velocity profile is recommended, where U_g, $u^\star$, y_g^+, and ν_g are the physical velocity, friction velocity, axial distance from the interface, and kinematic viscosity, all within the gas core:

$$\frac{U_g(y_g^+)}{u^\star} = 2.44\ln\left(y_g^+\right) + 5 - \Delta B \tag{41}$$

$$u^\star = \sqrt{\frac{\tau_i}{\nu_g}} \tag{42}$$

$$\Delta B = 2.44\ln\left(1 + c_B\frac{\epsilon u^\star}{\nu_g}\right) \tag{43}$$

The similarity of this velocity profile to the branch of the above-cited UVP for $y^+ > 30$ is notable. The profile in the Hurlburt et al. model is primarily differentiated by use of a slightly different constant (2.44 rather than 2.5) in front of the logarithm. The offset due to roughness is the ΔB term. In this term, c_B is a constant obtained with experimental data. As examples, Hurlburt et al. claim that sand roughness and stationary, wavy wall data are fit by c_B values of 0.3 and 0.8, respectively.

In annular flow, the second term within the logarithm of Eq. (43) is dominant; ΔB is approximated as:

$$\Delta B \approx 2.44\ln\left(c_B\frac{\epsilon u^\star}{\nu_g}\right) \tag{44}$$

This permits analytical solution of the interfacial friction factor, $C_{f,i}$, for round tubes:

$$C_{f,i} = 0.58^2\left[-\frac{\ln\hat{\epsilon}}{(\hat{\epsilon}-1)^2} - \ln c_B + 1.05 + \frac{1}{2}\frac{\hat{\epsilon}+1}{\hat{\epsilon}-1}\right]^{-2} \tag{45}$$

$$\hat{\epsilon} = \frac{2\epsilon}{D-\delta} \tag{46}$$

The roughness parameter $\hat{\epsilon}$ is non-dimensionalized by the maximum gas core diameter, which is equal to the tube diameter less twice the minimum film thickness. This minimum film thickness is assumed to be one-half of the average. For the base film, the value of $c_{B,base}$ was 0.8, with $c_{B,wave}$ set to 4.7.

The fraction of measurements assigned to the wave zone is termed the wave intermittency, INT_w. The technique used for separation of measurements into base film and waves was discussed in Section 4 and varies from that in the original model. The average film thicknesses and corresponding roughnesses in each zone, for the tube data, are correlated using:

$$\delta_{base} = c_{HEA}\overline{\delta} + \epsilon_{base} \tag{47}$$

$$\epsilon_{base} = s(\delta) \tag{48}$$

$$\delta_{wave} = c_{HEA}\overline{\delta} + \epsilon_{wave} \tag{49}$$

$$\delta_{wave}INT_w + \delta_{base}(1 - INT_w) = \overline{\delta} \tag{50}$$

These revised equations include c_{HEA}, set to 0.5 in the original model, and enforce the overall average film thickness, $\overline{\delta}$ match that from the two zones, weighted by INT_w.

For the base film, the mean liquid velocity, $U_{l,base}$, interfacial shear, $\tau_{i,base}$, and mean gas velocity, $U_{g,base}$, are estimated by simultaneous solution of the following equations:

$$U_{l,base} = u^\star_{base}\left[\left(1.5\left(\delta^+_{base}\right)^{\frac{2}{3}}\right)^{-2} + \left(9.5\left(\delta^+_{base}\right)^{0.1}\right)^{-2}\right]^{-0.5} \tag{51}$$

$$u^\star_{base} = \sqrt{\frac{\tau_{i,base}}{\rho_l}} \tag{52}$$

$$\delta^+_{base} = \frac{\delta_{base}u^\star_{base}}{\nu_l} \tag{53}$$

$$\tau_{i,base} = 0.5C_{f,i,base}\rho_g\left(U_{g,base} - U_{l,base}\right)^2 \tag{54}$$

$$U_{g,base} = U_{sg}\left(\frac{D}{D_{core,base}}\right)^2 \tag{55}$$

$$D_{core,base} = D - 2\delta_{base} \tag{56}$$

Eq. (51) combines the laminar film model of Asali et al. (1985) (first term within square brackets) and the turbulent film model of Henstock and Hanratty (1976) (second term) to estimate the interfacial velocity.

Calculation in the wave zone is very similar, with the Henstock and Hanratty relation used exclusively:

$$U_{l,wave} = u^{\star}_{wave}\left(9.5\left(\delta^{+}_{wave}\right)^{0.1}\right) \quad (57)$$

$$u^{\star}_{wave} = \sqrt{\frac{\tau_{i,wave}}{\rho_l}} \quad (58)$$

$$\delta^{+}_{wave} = \frac{\delta_{wave} u^{\star}_{wave}}{\nu_l} \quad (59)$$

$$\tau_{i,wave} = 0.5 C_{f,i,wave} \rho_g \left(U_{g,wave} - U_{l,wave}\right)^2 \quad (60)$$

$$U_{g,wave} = U_{sg}\left(\frac{D}{D_{core,wave}}\right)^2 \quad (61)$$

$$D_{core,wave} = D - 2\delta_{wave} \quad (62)$$

The correlated average interfacial shear is then found by:

$$\tau_{i,HEA} = (1 - INT_w)\tau_{i,base} + INT_w \tau_{i,wave} \quad (63)$$

This correlated result is compared to the same experimental interfacial shear as was used for the Wallis correlation.

By providing average film flow velocities in both zones (Eqs. (51) and (57)), Hurlburt et al. have, in effect, provided film flow rates. These are summed, weighted by intermittency:

$$\dot{m}_{l,film} = INT_w \dot{m}_{l,film,wave} + (1 - INT_w)\dot{m}_{l,film,base} \quad (64)$$

$$\dot{m}_{l,film,base} = U_{l,i,base} \pi D \rho_l \delta_{base} \quad (65)$$

$$\dot{m}_{l,film,wave} = U_{l,i,wave} \pi D \rho_l \delta_{wave} \quad (66)$$

The values of all quantities relating to entrainment were estimated in the same manner as for the Wallis model (using a liquid mass balance, assuming droplet and gas velocities are equal in the core, and using the relation suggested by Ishii for droplet deposition flux, R_D). As was the case for the Wallis correlation, the accuracy of the Hurlburt et al. model is only weakly dependent on these details.

Providing the average film velocity as a function of δ^+ provides a film velocity profile. The velocity at the top of the waves (the wave velocity, v_{wave}) is found to be

$$v_{wave} = u^{\star}_{wave}\left(10.45\left(\delta^{+}_{wave}\right)^{0.1}\right) \quad (67)$$

Application of the Hurlburt et al. model requires film thickness distribution data and flow rates. It produces an estimate of interfacial shear, easily convertible to wall shear or pressure loss, and (secondarily) estimates of v_{wave} and E.

5.2. Performance of Hurlburt et al. model

The time-averaged shear at the gas–liquid interface, τ_i, is selected as the primary parameter of comparison. This is estimated from experimental data using Eq. (2). For the implementation of the model, as discussed above, the mean absolute error (MAE) is found to be 33%, inferior to that from the Owen and Hewitt single-zone model. Fig. 8 shows the predictions of the Hurlburt et al. model for interfacial shear and entrainment as functions of flow rate. Scatterplots of the modeled interfacial shear with the experimental estimate are also shown.

The effect of liquid flow on τ_i (particularly at low gas flow) is underestimated, while the effect of gas flow is overestimated. The modeled entrained fraction, E, is only a very weak function of gas flow. A stronger liquid flow effect is seen, particularly at low liquid flow (U_{sl} of 6.3 cm s^{-1}). The Ishii and Mishima correla-

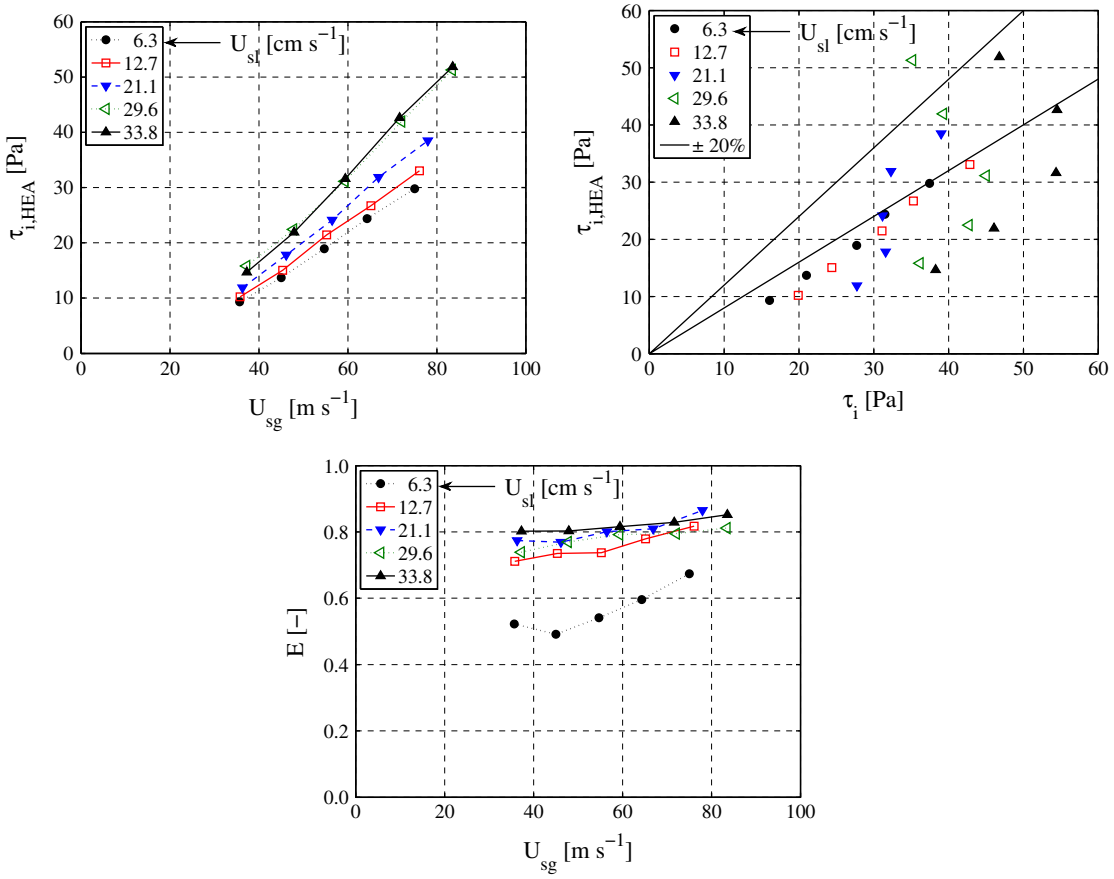

Fig. 8. Results from Hurlburt et al. model, using entrainment estimates from liquid mass balance and INT_w data from wave visualization, series of constant U_{sl}. (Top left) $\tau_{i,HEA}$ vs. flow rates. (Top right) $\tau_{i,HEA}$ vs. τ_i from Eq. (2). (Bottom) E vs. flow rates.

tion shows a stronger gas flow rate effect. Since the liquid-phase mass balance does not produce results consistent with experiment, it is unlikely that the film flow rate expressions (implied film velocity profiles) in the work of Hurlburt et al. are accurate for vertical annular air–water flow.

The original paper uses $c_{B,wave}$ as a fitting factor, setting $c_{B,base}$ to 0.8 to agree with stationary wavy wall data and, by extension, the base film. An increase in $c_{B,wave}$ will increase $\tau_{i,wave}$ throughout the data set, with low U_{sg} and high U_{sl} flows increased the most (when δ_{wave} and INT_w are large). A $c_{B,wave}$ of 9.4 improves the MAE with respect to τ_i to 26%. This prediction is still somewhat inferior to the Owen and Hewitt model. Its results are shown in Fig. 9.

The value of $U_{l,i,wave}$ from the model can also be compared to the average wave velocity, v_{wave}, from experimental data. In doing so, both the change in diameter must be considered. Based on results in Schubring et al. (2010) and Schubring and Shedd (2008) wave velocity at constant mass flow rates can be expected to increase by approximately 7% with a diameter change from 23.4 mm to 22.4 mm. The MAE for the estimate of wave velocity is found to be 8%, with no strong mean error. Fig. 10 shows the predicted wave velocities and the relation between these predictions and wave video results. Comparison of v_{wave} to the average liquid film velocity in the wave zone ($U_{l,wave}$, Eq. (57)) was also attempted. An increase in MAE to 11% is observed, with most results underpredicted.

As a global model, this optimized version of Hurlburt et al. provides mixed results. The entrainment estimates obtained are a poor match with correlations from actual entrainment data. This may be linked to the base film velocity profile, for which no data from the present work are available. The interfacial shear (pressure loss) prediction is adequate for many purposes (especially low U_{sl}), but can be bettered by other, simpler correlations or the single-zone Owen and Hewitt model. The prediction for v_{wave} is the strongest result from the optimized Hurlburt et al. model, emphasizing the close link between pressure loss and wave behavior.

6. Conclusions and future work

Some conclusions can be drawn regarding the models considered and the division of film thickness data (from PLIF) between base film and waves:

- The simple one-zone Wallis correlation under-predicts the dependence of interfacial shear and pressure loss on liquid flow rate. Authors infer that a high liquid flow rate behavior (such as waves or entrainment) is not adequately modeled by this relation.
- The Owen and Hewitt model can be rephrased to provide estimates of pressure loss and entrainment given film thickness. This model over-predicts the dependence of dP/dx on gas flow rate for high liquid flow conditions.
- When both pressure loss and film thickness are supplied to the model, the relation between average film thickness, δ, and roughness, ϵ, can be explored. For the current experimental data, this relationship must be a function of liquid flow for all gas flows. Additional roughness (at the same average film thickness) is required for higher liquid flow series; authors suggest that this additional roughness may be linked to disturbance waves.

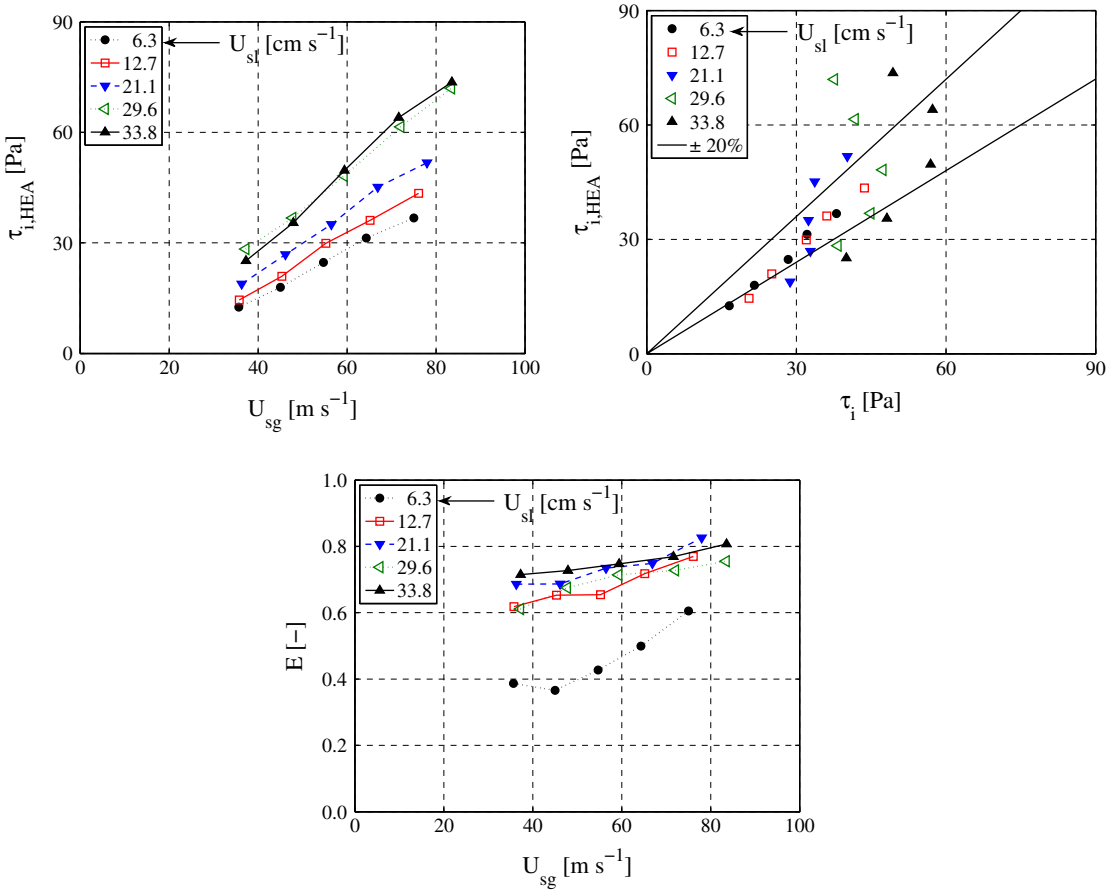

Fig. 9. Results from Hurlburt et al. model with $c_{B,wave}$ optimized, series of constant U_{sl}. (Top left) $\tau_{i,HEA}$ vs. flow rates. (Top right) $\tau_{i,HEA}$ vs. τ_i from Eq. (2). (Bottom) E vs. flow rates.

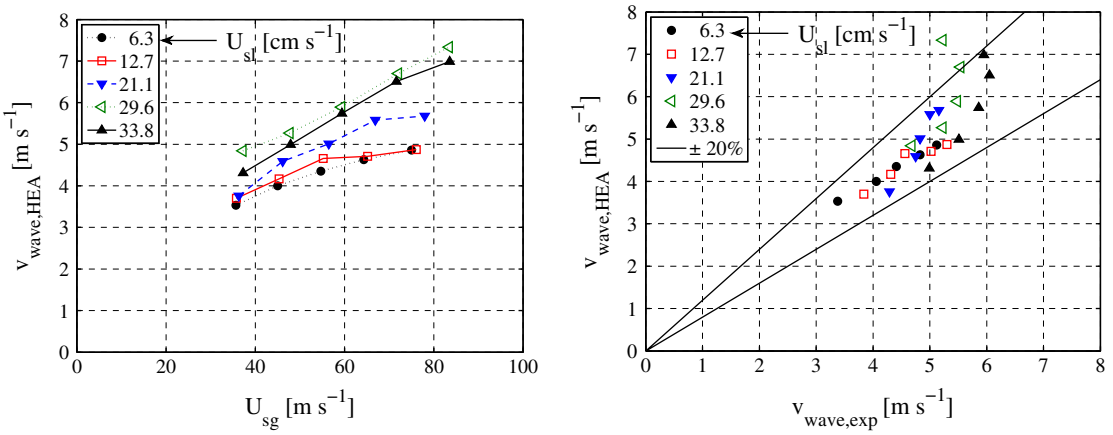

Fig. 10. Results from Hurlburt et al. model pertaining to wave velocity. (Left) Predicted v_{wave} as a function of flow rates. (Right) Comparison with results from high-speed video analysis.

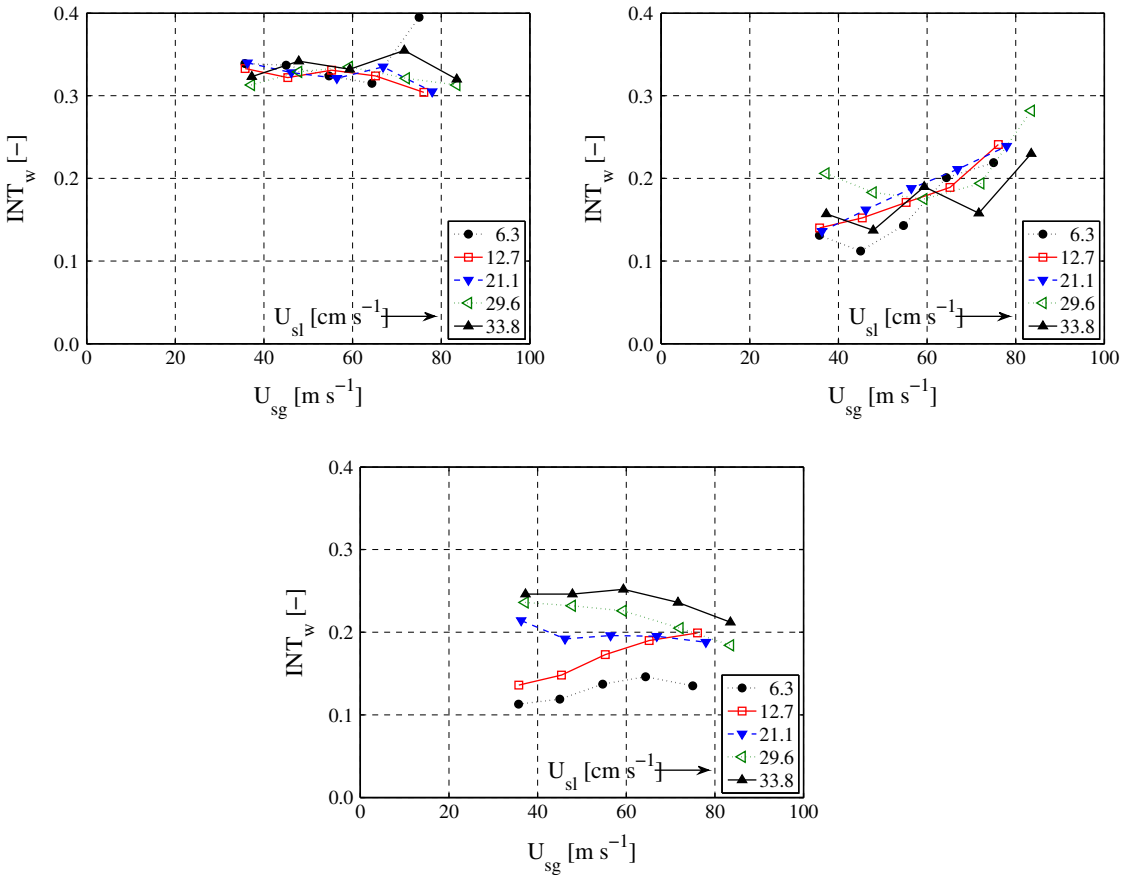

Fig. 11. Estimates of wave intermittency. (Top left) From method of Hurlburt et al. (Top right) From k_c method. (Bottom) From wave visualization.

- Both the critical standard deviation multiplier method of Rodríguez (2004) and the 1.1 times average criterion of Hurlburt et al. (2006) appear inadequate for dividing base film thickness from wave heights. An estimate of INT_w from parallel work was used to produce reasonable results, but base/wave division based only on film thickness distribution data remains elusive.
- The Hurlburt et al. model provides an estimate of pressure loss given film thickness and wave intermittency. It can be extended to estimate entrainment and wave velocity.
- Even if the empirical constant in the wave-zone friction factor is adjusted, the high liquid flow trends of the interfacial shear from the model do not agree with experiment. In contrast to the Wallis model, the work of Hurlburt et al. over-predicts the dependence of τ_i in such flows on gas flow rate.
- The entrainment estimates from the modeled shear, film flow rates, and mass conservation do not agree with trends from direct studies of entrainment.

- The accuracy of the estimate of v_{wave} from the Hurlburt et al. model is comparable to that from direct empirical wave velocity correlations.

Based on the results in this work (Parts I and II), two main branches of future work are advised. The first is application of the planar laser-induced fluorescence film thickness measurement itself to other annular flow conditions. Application to horizontal, inclined, and developing flows, including those with different mechanisms of gas–liquid mixing, is an obvious first use of PLIF to characterize adiabatic annular flow. Annular flows with heat transfer are predominant in industrial applications and future work on such conditions is advisable.

The second area is improvement of the modeling of annular flow. Little quantitative information is available regarding film velocity profiles; detailed results in this area are essential to modeling the transport of liquid mass. The Owen and Hewitt (single-zone) and Hurlburt et al. (two-zone) models both under-predict the importance of liquid flow rate on pressure loss and interfacial shear. Since wave activity and entrained liquid flow rate both increase with increased liquid flow, it is likely that the treatment of one of these mechanisms of liquid mass transport is incomplete. A more detailed model of disturbance waves is likely to include their dynamic charcteristics (velocity, frequency, etc.) and/or an explicit characterization of the behavior of the gas core across the transition from base film to waves.

Acknowledgement

The financial support of Bettis Laboratory is gratefully acknowledged.

References

Asali, J.C., 1984. Entrainment in vertical gas–liquid annular flows. PhD thesis, University of Illinois at Urbana-Champaign, Urbana, IL, USA.

Asali, J.C., Hanratty, T.J., Andreussi, P., 1985. Interfacial drag and film height for vertical annular flow. AIChE Journal 31, 895–902.

Azzopardi, B.J., 1986. Disturbance wave frequencies, velocities and spacing in vertical annular two-phase flow. Nuclear Engineering and Design 92, 121–133.

Azzopardi, B.J., 1997. Drops in annular two-phase flow. International Journal of Multiphase Flow 23, 1–53.

Chisholm, D., 1973. Pressure gradients due to friction during the flow of evaporating two-phase mixtures in smooth tubes and channels. International Journal of Heat and Mass Transfer 16, 347–358.

Fore, L.B., Beus, S.G., Bauer, R.C., 2000. Interfacial friction in gas–liquid annular flow: analogies to full and transition roughness. International Journal of Multiphase Flow 26, 1755–1769.

Haaland, S.E., 1983. Simple and explicit formulas for the friction factor in turbulent pipe flow. Journal of Fluids Engineering 105, 89–90.

Han. H., 2005. A Study of Entrainment in Two-Phase Upward Cocurrent Annular Flow in a Vertical Tube. PhD thesis, University of Saskatchewan, Saskatoon, Saskatchewan, Canada.

Hay, K.J., Liu, Z., Hanratty, T.J., 1996. Relations of deposition to drop size when the rate law is nonlinear. International Journal of Multiphase Flow 22, 829–848.

Henstock, W.H., Hanratty, T.J., 1976. The interfacial drag and the height of the wall layer in annular flows. AIChE Journal 22, 990–1000.

Hewitt, G.F., Hall Taylor, N.S., 1970. Annular Two-Phase Flow. Pergamon Press, Oxford, UK.

Hewitt, G.F., Jayanti, S., Hope, C.B., 1990. Structure of thin liquid films in gas–liquid horizontal flow. International Journal of Multiphase Flow 16, 951–957.

Hurlburt, E.T., Fore, L.B., Bauer, R.C., 2006. A two zone interfacial shear stress and liquid film velocity model for vertical annular two-phase flow. In: Proceedings of the ASME Fluids Engineering Division Summer Meeting 2006, vol. 2, Miami, FL, USA, pp. 677–684.

Ishii M., Mishima, K., 1981. Correlation for liquid entrainment in annular two-phase flow of low viscous fluid. Argonne National Laboratory Report ANL/RA/LWR 81-2.

Jayawardena, S.S., 1993. Turbulent flow in the core region of vertical annular gas–liquid flow. PhD thesis, University of Houston, Houston, TX, USA.

Müller-Steinhagen, H., Heck, K., 1986. A simple friction pressure drop correlation for two-phase flow in pipes. Chemical Engineering Processing 20, 297–308.

Nedderman, R.M., Shearer, C.J., 1964. Correlation for the friction factor and velocity profile in the transition region for flow in and roughened pipes. Chemical Engineering Science 19, 423–428.

Owen, D.G., Hewitt, G.F., 1987. An improved annular two-phase flow model. In: 3rd International Conference on Multi-Phase Flow, The Hague, Netherlands, pp. 73–84.

Rodríguez, D.J., 2004. Characterization of bubble entrainment, interfacial roughness and the sliding bubble mechanism in horizontal annular flow. PhD thesis, University of Wisconsin-Madison, Madison, WI, USA.

Sawant, P., Ishii, M., Mori, M., 2008. Droplet entrainment correlation in vertical upward co-current annular two-phase flow. Nuclear Engineering and Design 238, 1342–1352.

Sawant, P., Ishii, M., Hazuki, T., Takamasa, T., Mori, M., 2008. Properties of disturbance waves in vertical annular two-phase flow. Nuclear Engineering and Design 238, 3528–3541.

Schadel, S., 1988. Atomization and deposition rates in vertical annular two-phase flow. PhD thesis, University of Illinois at Urbana-Champaign, Urbana, IL, USA.

Schubring, D., Shedd, T.A., 2008. Wave behavior in horizontal annular air–water flow. International Journal of Multiphase Flow 34, 636–646.

Schubring, D., Ashwood, A.C., Shedd, T.A., Hurlburt, E.T., submitted for publication. Planar laser-induced fluorescence (PLIF) measurements of liquid film thickness in annular flow. Part I: methods and data. International Journal of Multiphase Flow.

Schubring, D., Shedd, T.A., Hurlburt, E.T., 2010. Studying disturbance waves in vertical annular flow with high-speed video. International Journal of Multiphase Flow 36, 385–396.

Wallis, G.B., 1969. One-dimensional Two-phase Flow. McGraw-Hill, Inc., New York, NY, USA.

Wang, Z., Gabriel, K.S., Manz, D.L., 2004. The influences of wave height on the interfacial friction in annular gas–liquid flow under normal and microgravity conditions. International Journal of Multiphase Flow 30, 1193–1211.